Supporting Information for

J-aggregates Squaraine Nanoparticles with Bright NIR-II Fluorescence for Imaging Guided Photothermal Therapy

Pengfei Sun, [a†] Qi Wu, [a†] Xiaoli Sun, [a] Han Miao, [b] Weixing Deng, [a] Wansu Zhang, [a] Quli Fan *[a] and Wei Huang [c]

[a] Key Laboratory for Organic Electronics and Information Displays & Jiangsu Key Laboratory for Biosensors, Institute of Advanced Materials (IAM), Jiangsu National Synergetic Innovation Center for Advanced Materials (SICAM), Nanjing University of Posts & Telecommunications, 9 Wenyuan Road, Nanjing 210023, China.

[b] School of Materials Science and Engineering, Georgia Institute of Technology, Atlanta, GA 30332, USA.

[c] Shaanxi Institute of Flexible Electronics (SIFE), Northwestern Polytechnical University (NPU), 127 West Youyi Road, Xi'an 710072, Shaanxi, China.

[†] These authors contributed equally to this work

1. Experiments

1.1 Materials.

All starting materials and organic solvents were obtained from commercial suppliers and no further purification was performed. Hydroquinone, 1-bromododecane (98%), triethylphosphate (99%) and paraformaldehyde were obtained from Shanghai Aladdin biochemical technology Co., Ltd. (Shanghai, China). Hydrogen bromide (HBr, 41%) was purchased from J&K Scientific Ltd. (Sunnyvale, CA, USA). N-

Methylpyrrole-2-carboxaldehyde (98%), 3, 4-Dihydroxy-3-cyclobutene-1, 2-dione (99%) and Pluronic® F-127 were purchased from Sigma-Aldrich. NIR-II imaging depth material was chicken obtained from supermarket. MCF-7 cells were obtained from the Shanghai Laboratory Animal Center, Chinese Academy of Science (SLACCAS). The Annexin V-FITC/propidium iodide (PI) cell apoptosis kit were obtained from KeyGen Biotech. Co., Ltd (Nanjing, China). Dulbecco's modified Eagle's medium (DMEM, Gibco, U.S.) was purchased from Gene Tech Co. (Shanghai, China).

1.2 Characterization.

The ^{1}H NMR (400 MHz) spectra was obtained with a Bruker Ultra Shield Plus 400 MHz spectrometer, the apparatus use tetramethylsilane (TMS) as the internal standard and $CDCl_3$ as the solvent at 298 K. Dynamic light scattering (DLS) analysis were measured by a commercial light scattering spectrometer (ALV/CGS-3; ALV, Langen, Germany) outfit with a multi-τ digital time correlator (ALV-7004; ALV, Langen, Germany) and a He-Ne laser at λ = 632.8 nm). A CONTIN analysis was used for educe the $<R_h>$ data (from the scattering intensity). All samples were made optically clean by filtration though 0.45 μm Millipore filters before test and measured each sample for three times. The scattering angle was 90° and all measurements were conducted at 25.0 ± 0.5 °C. For all the samples, the final concentration of SQP-NPs$_{(J)}$ and SQP-NPs$_{(H)}$ were 0.1 mg mL^{-1}. The morphology of nanoparticles were investigated using HT7700 transmission electron microscope, the acceleration voltage is 100kV. The Formvar-graphite-coated copper grids (300 mesh, Electron Microscopy Science) were used to hold aqueous solution (0.1 mg mL^{-1}) of samples. The UV-vis-NIR

absorption spectra were recorded on a Shimadzu UV-3600 spectrophotometer at 25.0 ± 0.5 °C. The fluorescence spectra were monitored on a NIR-II spectroscopy (Fluorolog 3 Horiba) with InGaAs NIR detector under 808 nm diode laser excitation at room temperature. After raw emission data acquisition, the fluorescence spectra was further corrected accounting to the detector sensitivity profile. The 808 nm laser was purchased from Changchun New Industries Optoelectronics Technology Co., Ltd. The FT-IR spectra were measured by a Perkin-Elmer Model 882 infrared spectrometer. All photothermal tests were conducted by Fotric 225 (IR thermal camera, ± 2 °C), which was purchased from Fotric. (Shanghai, China). The methyl thiazolyl tetrazolium (MTT) assay were studied by a PowerWave XS/XS2 microplate spectrophotometer (BioTek, Winooski, VT). Flow cytometry experiments were investigated using a Flow Sight Imaging Flow Cytometer (Merck Millipore, Darmstadt, Germany). Cell imaging were detected by confocal laser scanning microscopy (CLSM) on an Olympus Fluoview FV1000 laser scanning confocal (Tokyo, Japen). The *in vivo* NIR-II fluorescence imaging was conduct on a home built NIR-II spectroscopy set-up from 900 nm to 1500 nm under the 808 nm laser excitation. The 808 nm laser was also purchased from Changchun New Industries Optoelectronics Technology Co., Ltd. The fluorescence signal were collected in the transmission geometry with a 980 nm long pass filter (ScmRock) to prevent the excitation light. The fluorescence image signal was detected by spectrometer (Acton SP2300i) equipped with an InGaAs camera (Princeton OMA-V).

1.3 Synthesis of SQP and related intermediates.

The synthetic routes toward related intermediates M1-M3 were shown in Supplementary Scheme 1. The detailed procedures of these intermediates and SQP were described below:

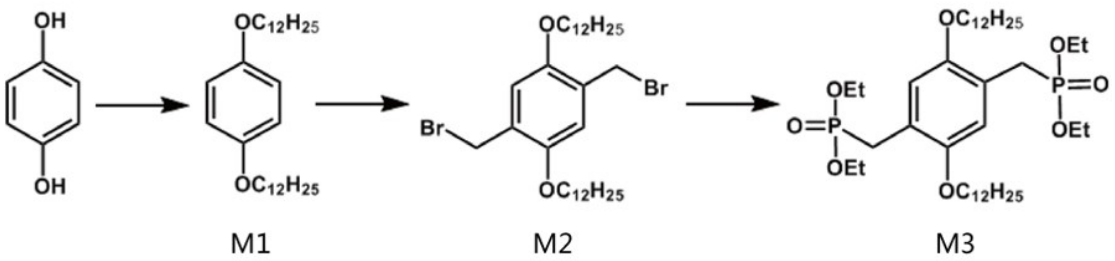

Supplementary Scheme 1: Synthesis of intermediates M1-M3.

(1) Preparation of M1:

Hydroquinone (4.4 g, 40 mmol), bromododecane (24.9 g, 100 mmol) and potassium carbonate (16.56 g, 120 mmol) were dissolved in 100 mL acetone and were refluxed for 24 h. After cooling, the reaction mixture was poured into cold water and the precipitate formed was collected by filtration. Recrystallization of the crude product from hot ethanol provided the M1 with the yield is 60%. ^{1}H NMR (400 MHz, $CDCl_3$, δ): 6.82 (s, 4 H), 3.90 (t, 4 H), 1.75 (m, 4 H), 1.4 (m, 4 H), 1.2 - 1.4 (m, 32 H), 0.88 (t, 6 H) ppm.

(2) Preparation of M2:

M1 (2.2 g, 5 mmol) and paraformaldehyde (0.6 g, 20 mmol) were dissolved in 80 ml glacial acetic acid under high vacuum. To this mixture, 41% of HBr (4 mL) was added and the reaction was refluxed for 24 h at 118 °C. After cooling, the reaction mixture was poured into cold water and extract with DCM. After removal of DCM under reduced pressure, Recrystallization of the crude product from hot ethanol

provided the M2 with the yield is 20%. ^{1}H NMR (400 MHz, $CDCl_3$, δ): 6.85 (s, 2 H), 4.53 (s, 4 H), 3.98 (t, 4 H), 1.81 (m, 4 H), 1.50 (m, 4 H), 1.2-1.4 (m, 32 H), 0.88 (t, 6 H) ppm.

(3) Preparation of M3:

Compounds M3 were prepared by the reaction of M2 (6.28 g, 10 mmol) with 5.0 mL of triethyl phosphite at 80 °C for 10 h followed by the removal of the unreacted triethyl phosphite under reduced pressure. The obtained product didn't need further purification and immediately input to next steps.

(4) Preparation of BP:

A suspension of sodium hydride (0.36 g, 15.0 mmol) in anhydrous tetrahydrofuran (THF) was added slowly to a solution of M3 (1.87 g, 2.5 mmol) and N-alkylpyrrole-2-carboxaldehyde (0.55 g, 5.0 mmol) in THF. After the reaction was refluxed for 12 h, a highly fluorescent mixture was obtained. Next, the THF was removed under reduced pressure to give a solid residue. This solid residue was suspended in water and extracted by dichloromethane. The organic layer was collected and dried over anhydrous sodium sulfate. The concentrated crude product was washed three times and precipitated by adding methanol to a dichloromethane solution. The pure product was obtained with a 26% yield. ^{1}H NMR (400 MHz, $CDCl_3$, δ): 7.14 (d, 2 H), 7.05 (d, 2 H), 6.97 (s, 2 H), 6.63 (s, 2 H), 6.48 (m, 2 H), 6.15 (t, 2 H), 4.01 (t, 4 H), 3.69 (s, 6 H), 1.84 (m, 4 H), 1.51 (m, 4 H), 1.26 (m, 32 H), 0.88 (t, 6 H) ppm.

(5) Preparation of SQP:

BP (0.197 g, 0.3 mmol) and squaric acid (0.0171 g, 0.15 mmol) in n-butanol/methylbenzene (1:3, 50 mL) were refluxed at 112 °C in a 1:2 stoichiometric ratio. The reaction mixture absorption spectra was frequently monitored, and the reaction was stopped when the absorption of higher molecular weight homologues (850 nm) start to appear. After the dark green reaction mixture was cooled, the n-butanol and methylbenzene were removed under reduced pressure to give a viscous solution. To remove the unreacted BP, the resultant dark green viscous solution was dissolved in dichloromethane, and the product was precipitated by adding light petroleum ether and washing with diethyl ether. After three re-precipitations and washing with petroleum ether and diethyl ether, the product was obtained at a 13% yield. ^{1}H NMR (400 MHz, CDCl3, δ): 7.77 (s, 2H), 7.4 (s, 2H), 7.17-7.10 (m, 6H), 6.92 (m, 6H), 6.63 (s,2H), 6.51 (s, 2H),6.16 (s,2H), 4.22 (s,6H), 4.04 (s, 6H), 3.48-3.67 (m, 8H), 1.85 (s, 8H), 1.63 (m, 8H), 1.25 (m, 32H), 1.03 (m, 6H).

1.4 Preparation of water-soluble nanoparticles.

(1) Preparation of SQP-NPs$_{(J)}$.

We dissolved SQP in tetrahydrofuran (THF) at a concentration of 0.5 mg mL^{-1} and dissolved F-127 in water at a concentration of 3.0 mg mL^{-1}. The ratio of SQP to F-127 was 1:15. Subsequently, the SQP organic solution was rapidly poured into the F-127 aqueous solution with sonication. The THF was then removed by complete evaporation in an airing chamber, with stirring at 40 °C. Finally, the green SQP-NPs$_{(J)}$ aqueous solution was obtained. The tubular ultrafiltration modules were used to remove the

excess F-127 aqueous solution until the SQP-NPs$_{(J)}$ aqueous solution was enriched to a concentration of 2.0 mg mL^{-1}.

(2) Preparation of SQP-NPs$_{(H)}$.

We dissolved SQP in dichloromethane (DCM) at a concentration of 0.5 mg mL^{-1} and dissolved F-127 in water at a concentration of 3.0 mg mL^{-1}. The ratio of SQP to F-127 was 1:15. Subsequently, the SQP organic solution was rapidly poured into the F-127 aqueous solution with sonication. The DCM was then removed by complete evaporation in an airing chamber, with stirring at 40 °C. Finally, the green SQP-NPs$_{(H)}$ aqueous solution was obtained. The tubular ultrafiltration modules were used to remove the excess F-127 aqueous solution until the SQP-NPs$_{(H)}$ aqueous solution was enriched to a concentration of 2.0 mg mL^{-1}.

(3) Preparation of IR1061-NPs.

We dissolved IR1061 in dichloromethane (DCM) at a concentration of 0.5 mg mL^{-1} and dissolved F-127 in water at a concentration of 3.0 mg mL^{-1}. The ratio of IR1061 to F-127 was 1:15. Subsequently, the IR1061 organic solution was rapidly poured into the F-127 aqueous solution with sonication. The DCM was then removed by complete evaporation in an airing chamber, with stirring at 40 °C. Finally, the green IR1061-NPs aqueous solution was obtained. The tubular ultrafiltration modules were used to remove the excess F-127 aqueous solution until the IR1061-NPs aqueous solution was enriched to a concentration of 2.0 mg mL^{-1}.

1.5 *In vitro* photothermal conversion efficiency.

The photothermal conversion efficiency (η) was calculated according to a previously described equation[1]. In a typical experiment, a 200 μL aqueous dispersion of SQP-NPs$_{(J)}$ (0.1 mg mL^{-1}) was added to a centrifuge tube and illuminated by an 810 nm LED lamp (1.5 W cm^{-2}) for 6 min. The LED lamp (PLS-LED100) was purchased from Beijing Poffei Technology Co., Ltd. The temperature changes were monitored by an infrared thermal camera (Fotric 225, Shanghai, China) and were recorded every 20 s throughout the laser irradiating time and cooling time. According to the obtained data and equation, the photothermal conversion efficiency of the SQP-NPs$_{(J)}$ was determined to be 36%.

1.6 Cell culture and cytotoxicity assay.

MCF-7 breast cancer cells were cultured at 37 °C in Dulbecco's modified Eagle's medium (DMEM) containing 10% fetal bovine serum with a humidified 5% CO_2 environment. *In vitro* cytotoxicity of the SQP-NPs$_{(J)}$ was determined in MCF-7 cells by the MTT assay. MCF-7 cells were cultured in DMEM on a 96-well plate for 24 h, and 2×10^4 cells were seeded per well. The cells were cultured in medium supplemented with different doses of SQP-NPs$_{(J)}$ for an additional 24 h. The concentration of NPs in the culture medium ranged from 0 to 100 mg mL^{-1}. Formazan crystals were produced following the addition of 20 μL of 3-(4,5-dimethyl-2-thiazolyl)-2,5-diphenyl-2-tetrazolium bromide (MTT) (5.0 mg mL^{-1}) solution to each well and incubation for 4 h at 37 °C. Next, the upper supernatant was removed, the formazan crystals were lysed with 200 μL of DMSO and the plate was shaken for 10 min to completely mix the samples. The absorbance was then evaluated at 490 nm using a PowerWave XS/XS2

microplate spectrophotometer. The absorption of the untreated cells was used as a control, and its absorption value was used as the reference value for calculating 100% cellular viability.

1.7 *In vitro* phototoxicity assay.

MCF-7 cells were cultured in DMEM in a 96-well plate for 24 h, and 2×10^4 cells were seeded per well. Next, the cells were cultured in the medium supplemented with different doses of SQP-NPs$_{(J)}$ for 4 h in the dark. The concentration of NPs in the culture medium ranged from 0 to 100 mg mL^{-1}. The SQP-NPs$_{(J)}$ mixture suspensions were replaced by fresh DMEM, and the selected wells were illuminated by an 808 nm LED lamp (0.8 W cm^{-2}, 10 min). After an additional 24 h of incubation, formazan crystals were produced by the addition of 20 μL of MTT solution (5.0 mg mL^{-1}) to each well and incubation for 4 h at 37 °C. The upper supernatant was then removed, the formazan crystals were lysed with 200 μL of DMSO, and the plate was shaken for 10 min to completely mix the samples. Cell viability was calculated by the absorbance at 490 nm using a PowerWave XS/XS2 microplate spectrophotometer. The absorption of the untreated cells was used as a control, and its absorption value was used as the reference value for calculating 100% cellular viability.

1.8 Assessment of the photothermal effect *in vitro* by Flow cytometry.

MCF-7 cells were cultured in DMEM and were seeded into 6-well plates until the cell population increased to 1×10^5 cells mL^{-1} per well. SQP-NPs$_{(J)}$ were added to the fresh DMEM medium to obtain the mixture medium (0.1 mg mL^{-1}). After the MCF-7 cells incubated with this mixture medium for 4 h in the dark, the SQP-NPs$_{(J)}$ mixture

suspensions were removed and were replaced by fresh DMEM. Next, the selected wells were illuminated by an 808 nm LED lamp (0.8 W cm^{-2}) for 10 min. After 24 h apoptosis, the MCF-7 cells that detached from 6-well plates were washed twice with PBS. Annexin V-FITC/PI dye solution was added to the collected cells for staining, and the cells were tested by flow cytometry.

1.9 Assessment of the photothermal effect *in vitro* by confocal imaging.

MCF-7 cells were seeded in CLSM culture dishes (Costar) until the cell population increased to 1×10^5 cells mL^{-1}. The SQP-$NPs_{(J)}$ were then added to the DMEM medium to obtain the mixture medium (0.1 mg mL^{-1}). After MCF-7 cells incubated with this mixture medium for 4 h in the dark, the SQP-$NPs_{(J)}$ mixture suspensions were removed and were replaced by a fresh DMEM. Next, the selected culture dishes were illuminated by an 808 nm LED lamp (0.8 W cm^{-2}) for 10 min. After 24 h apoptosis, the cells were washed twice to remove the cell debris and were then incubated with calcein-AM/propidium iodide (PI) dye solution for 10 min. Finally, the cells were imaged by CLSM (Olympus Fluoview FV1000).

1.10 Animals and tumor model.

All animal experiments were carried out in accordance with the NIH guidelines for the care and use of laboratory animals (NIH Publication no.85-23 Rev. 1985) and were approved by the Animal Ethics Committee of Simcere Bio Tech Corp., Ltd. Female BALB/c nude mice (age 5-6 weeks) were obtained from the Shanghai Laboratory Animal Center, Chinese Academy of Science (SLACCAS). MCF-7 tumors were established by subcutaneous injection of MCF-7 cells suspended in 50 μL of PBS

(4×10^6) into the left armpit of mice. The tumor volume was measured as $V = 0.5\ LW^2$, where L and W refer to the longitudinal and transverse diameters of the tumor, respectively.

1.11 *In vivo* NIR-II Imaging.

The healthy BALB/c mice were intravenously injected with SQP-$NPs_{(J)}$ (100 μL, 2.0 mg mL^{-1}). The MCF-7 tumor-bearing mice were also intravenously injected with SQP-$NPs_{(J)}$ after the tumor volume reached approximately 100 mm^3. During the test processes, the mice were sedated by breathing isoflurane. The *in vivo* NIR-II fluorescence imaging was taken at different post-injection times on an in-house NIR-II spectroscopy setup from 900 nm to 1500 nm under the 808 nm excitation (50 mW cm^{-2}). The fluorescence measurements were collected in the transmission geometry with a 980 nm long pass filter to prevent excitation light. The SQP-$NPs_{(J)}$ aqueous solution was placed into a 1 mm path cuvette (Starna Cells, Atascadero, CA, USA) for irradiation. The fluorescence image signal was detected by a spectrometer equipped with an InGaAs camera.

1.12 *In vivo* photothermal therapy (PTT).

After the tumors of MCF-7-bearing mice reached approximately 100 mm^3, these mice were randomly divided into four groups (six mice per group). These mice received the following treatments: (i) saline (i.v. injection 100 μL), (ii) LED lamp, (iii) SQP-$NPs_{(J)}$ (i.v. injection 100 μL 2.0 mg mL^{-1}), (iv) SQP-$NPs_{(J)}$ (i.v. injection 100 μL 2.0 mg mL^{-1}) in combination with LED lamp. The tumor region of the selected illumination groups were exposed to the LED luminescence (808 nm 0.8 W cm^{-2}) for 10 min via the

tail vein of SQP-NPs$_{(J)}$ mice for 24 h. Meanwhile, an IR thermal camera was used to record the temperature change of the tumor sites. The weights of the tumors and body were also monitored every two days after intravenous injection. After 15 days, we sacrificed these mice and the tumors were collected. The harvested tumors were fixed in 4% neutral-buffered paraformaldehyde and were embedded with paraffin for hematoxylin-eosin (H&E) staining. The histological tumor sections were imaged using an optical microscope.

1.13 Hemolysis assay.

Blood samples were harvested from healthy BALB/c mice, and ethylenediaminetetraacetic acid (EDTA) (anticoagulant) was added for stabilization. Approximately 1.0 mL of blood sample was diluted with 5.0 mL of PBS and was centrifuged at 1200 rpm for 10 min. The sample was then placed at room temperature for 2 h until the red blood cells (RBCs) and blood plasma separated. After repeated washing with PBS, followed by diluting with 10 mL of PBS, 0.3 mL of diluted RBCs were mixed with (i) 1.2 mL of PBS as a negative control, (ii) 1.2 mL of deionized water as a positive control, and (iii) 1.2 mL of SQP-NPs$_{(J)}$ with different concentration (0-0.8 mg mL^{-1}). All of the mixtures were shaken and then allowed to sit for 4 h at room temperature. After an additional 5 min centrifugation at 12000 rpm, the supernatants were collected and their absorbance at 541 nm was monitored by UV-vis spectroscopy. The hemolysis percent of RBCs was calculated by the following equation:

$$equation\ hemolytic\ efficiency = \frac{(A_{sample} - A_{negative\ control})}{(A_{positive\ control} - A_{negative\ control})} \times 100\% \quad \ldots\ldots\ldots\ldots\ldots\ldots (2)$$

where A_{sample}, $A_{positive}$ and $A_{negative}$ represent the absorption values of the samples, positive control and negative control, respectively.

1.14 Blood hematology and biochemistry analysis.

The BALB/c mice were randomly divided into two groups (n=3/group) and given the following treatments: i) saline (i.v. injection 200 μL), (ii) SQP-$NPs_{(J)}$ (i.v. injection 200 μL 2.0 mg mL^{-1}). The body weights of the mice were monitored. The blood samples were harvested from the fundus artery of group (ii) at 0, 7, and 30 days. EDTA was added to the collected blood samples as a stabilizer. Next, approximately 1 mL of blood diluted with 5 mL of PBS was centrifuged at 1200 rpm for 10 min and was placed at room temperature for 2 h until the red blood cells (RBCs) and blood plasma became separated. After repeated washing with PBS, the blood plasma was used for biochemical analysis. Renal function markers (CRE and BUN) and hepatic function markers (ALT and AST) were monitored, and routine blood tests were conducted.

1.15 Pathology analysis.

After injection with SQP-$NPs_{(J)}$ (2.0 mg mL^{-1}), the BALB/c mice were randomly divided into three groups (n=3/group). The three groups of mice were sacrificed 0, 7 and 30 days, respectively, to collect the main organs for H&E staining. These organs included the heart, spleen, lungs, kidneys and liver. The slices were tested using an inverted luminescence microscope.

2. Figures and discussion.

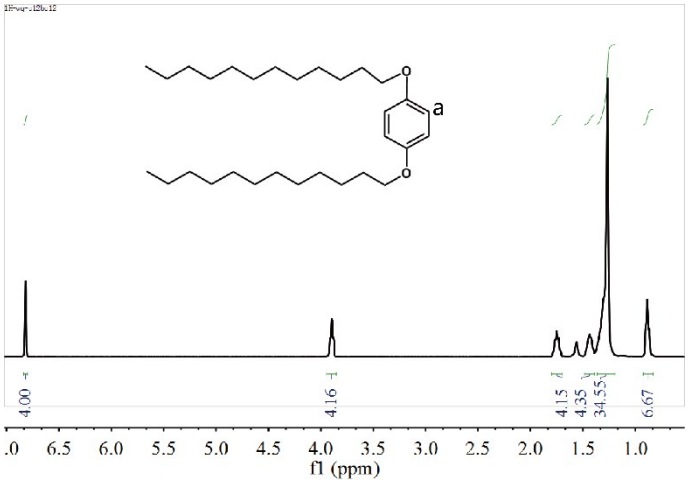

Figure S1. ^{1}H-NMR spectra of M1 in $CDCl_3$.

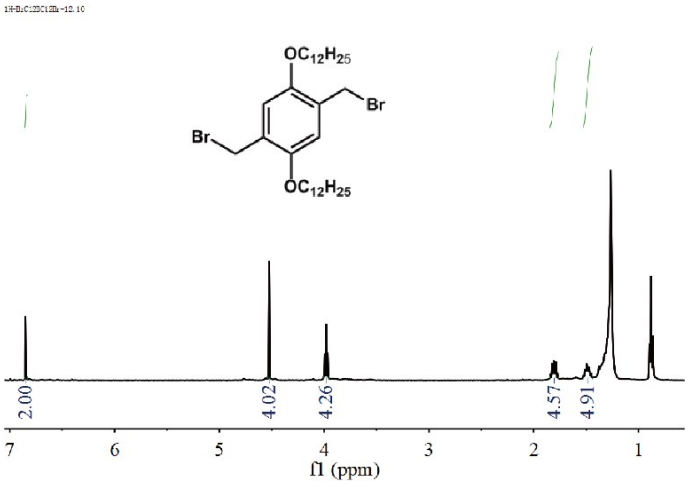

Figure S2. ^{1}H-NMR spectra of M2 in $CDCl_3$.

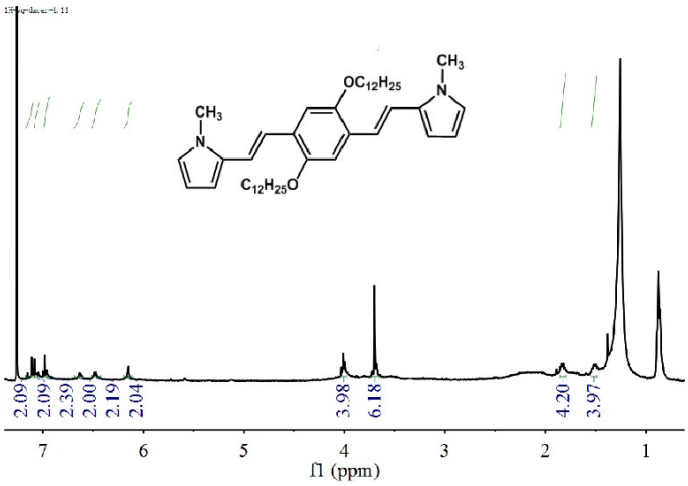

Figure S3. ^{1}H-NMR spectra of BP in $CDCl_3$.

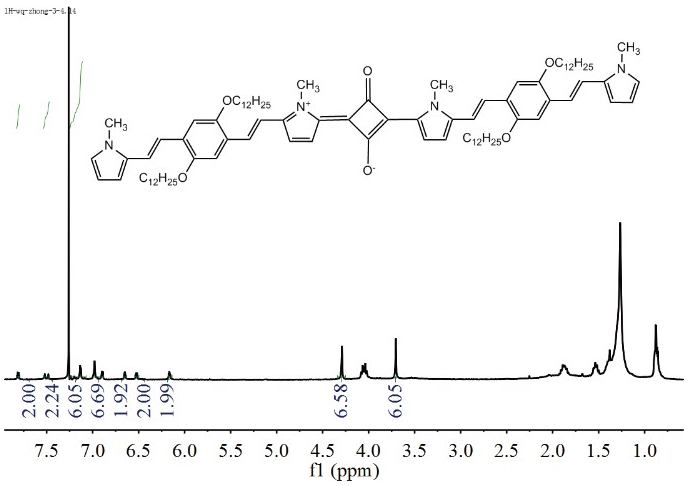

Figure S4. ^{1}H-NMR spectra of SQP in $CDCl_3$.

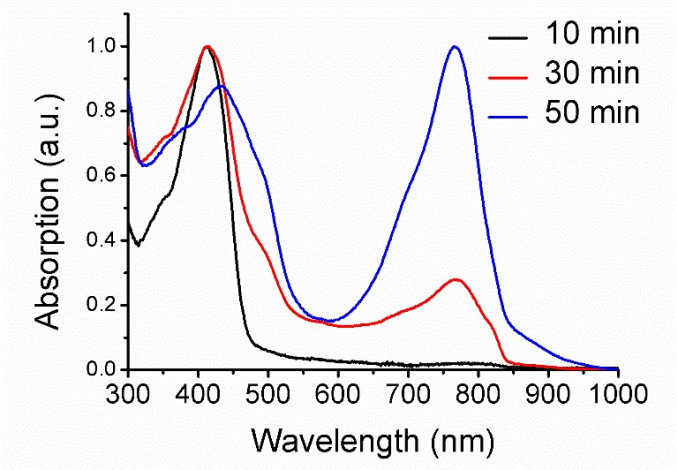

Figure S5. UV-vis-NIR absorption spectra change of the reaction of BP and squaric acid at different intervals.

The reaction time for prepare SQP was accurately controlled by monitoring the reaction mixture absorption spectrum, and the reaction stopped when the absorption of higher molecular weight homologues (850 nm) started to appear.

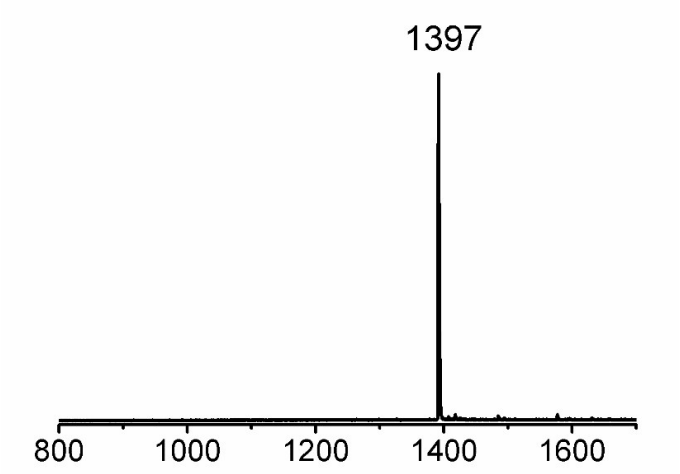

Figure S6. MALDI-TOF mass spectrometry of SQP.

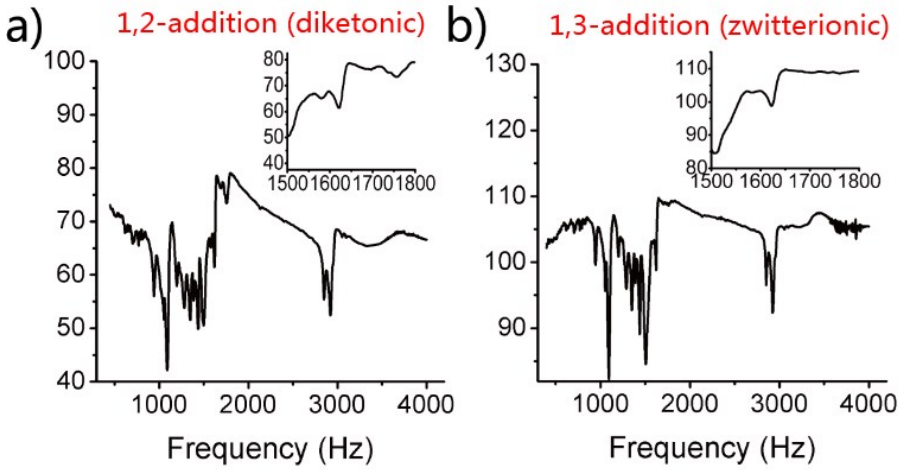

Figure S7. FT-IR spectra of two types repeating units of SQP.

The FTIR spectroscopic absorptions can identify two types of repeating units of SQP: 1,2-addition (diketonic) and 1,3-addition (zwitterionic).[2] 1,2-groups have one or two medium peaks at approximately 1750 cm^{-1}, and 1,3-groups should have peaks between 1620 and 1630 cm^{-1}. As shown in Figure S7, the FTIR spectra of SQP showed strong peaks between 1620 and 1630 cm^{-1}, but no peaks were seen at approximately 1750 cm^{-1}, which is the feature of the highly purified, resonance-stabilized 1,3-cyclobutanediolate dianion types of SQP.

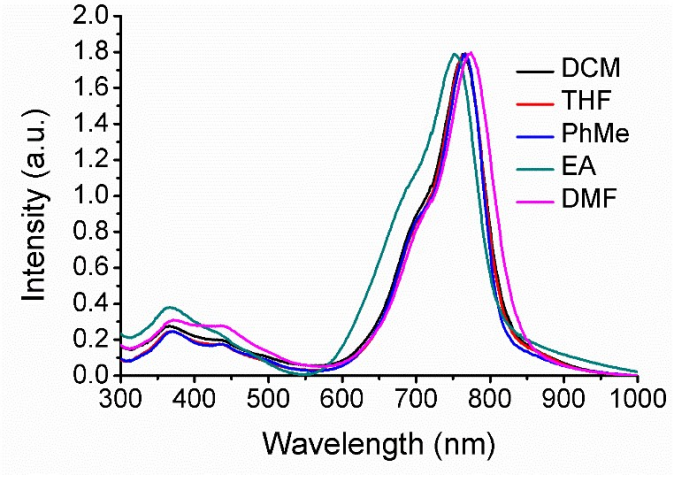

Figure S8. The absorption spectra of SQP in different solvents.

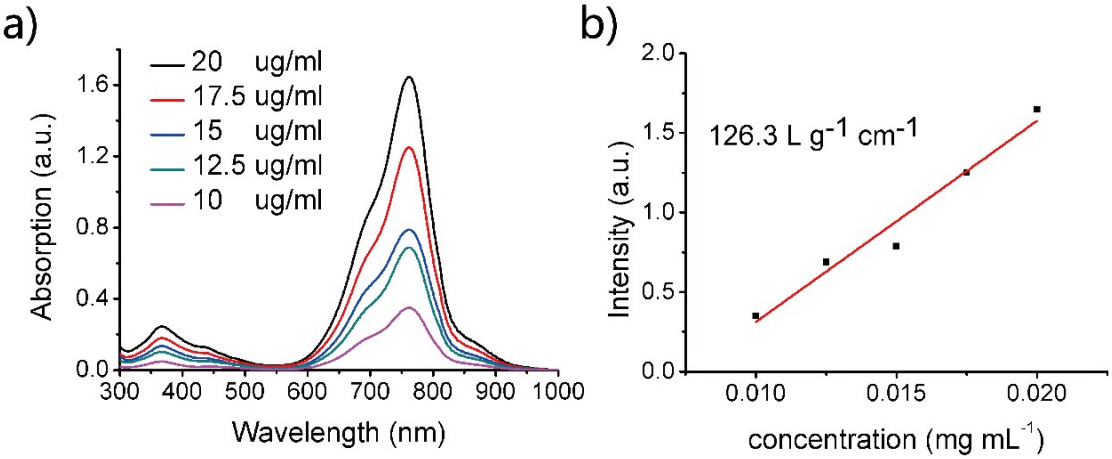

Figure S9. a) UV-vis-NIR spectra of SQP in THF at different concentration. b) The mole extinction coefficient of SQP at 765 nm.

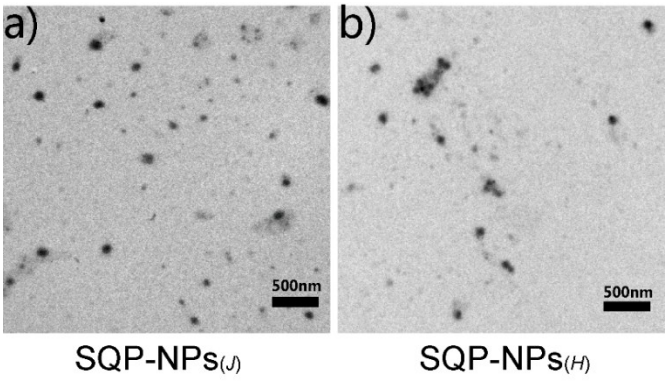

Figure S10. The TEM image of a) SQP-NPs$_{(J)}$ and b) SQP-NPs$_{(H)}$ in water.

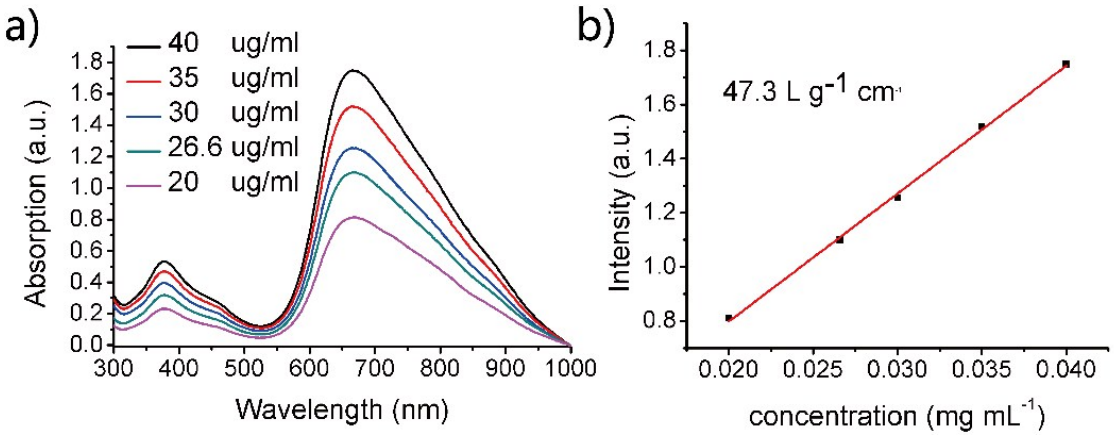

Figure S11. a) UV-vis-NIR spectra of SQP-NPs$_{(H)}$ in water at different concentration. b) The mole extinction coefficient of SQP-NPs$_{(H)}$ at 670 nm.

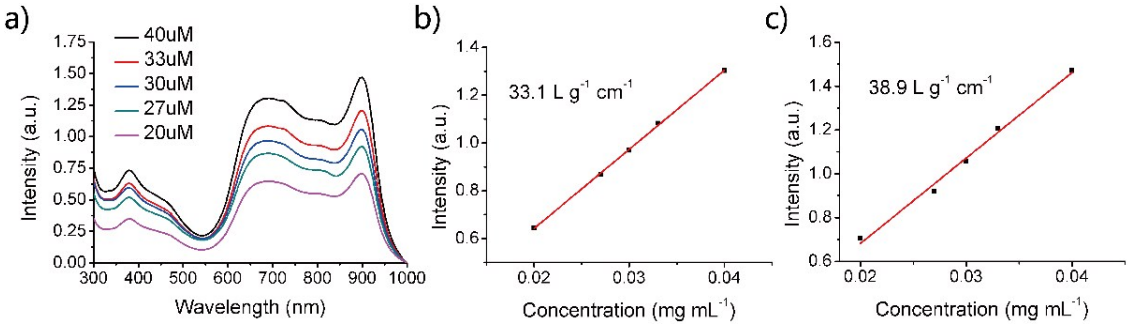

Figure S12. a) UV-vis-NIR spectra of SQP-NPs$_{(J)}$ in water at different concentration. b) The mole extinction coefficient of SQP-NPs$_{(J)}$ at 690 nm. c) The mole extinction coefficient of SQP-NPs$_{(J)}$ at 899 nm.

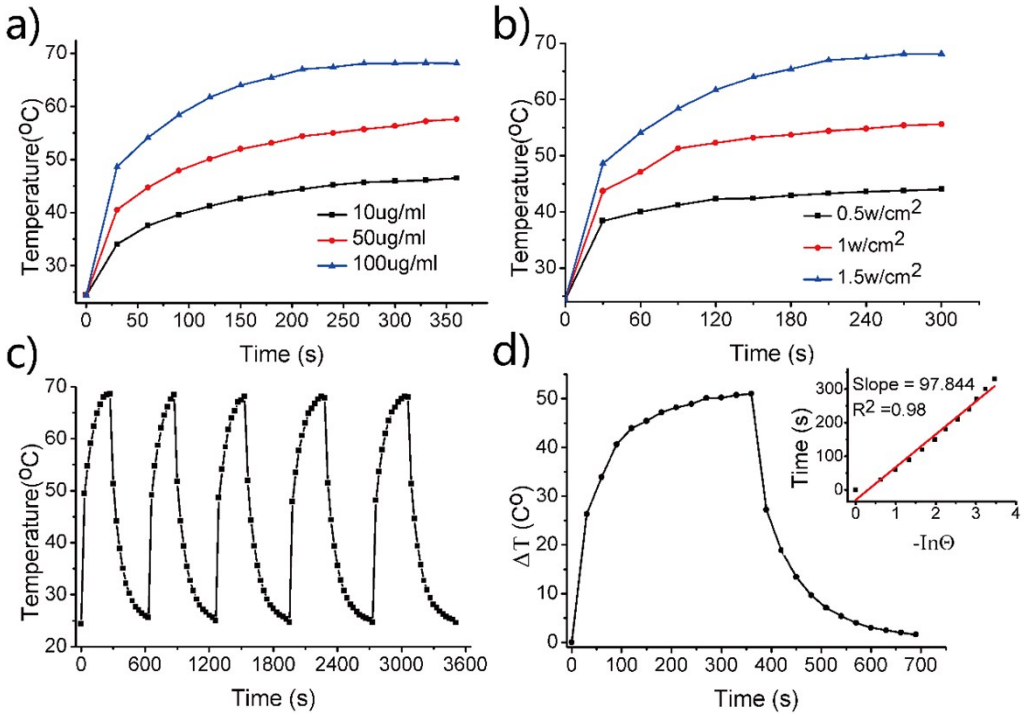

Figure S13. a) Temperature increase curves of SQP-NPs$_{(J)}$ with various concentration under 810 nm LED lamp (1.5 W cm^{-2}). b) Temperature increase curves of SQP-NPs$_{(J)}$ with various power density under 810 nm LED lamp at the concentraion of 100 μg mL^{-1}. c) Photothermal cycle curve of SQP-NPs$_{(J)}$ (100 μg mL^{-1}) which exposed to on/off LED lamp (810 nm 1.5 W cm^{-2}). d) Temperature change (ΔT) of SQP-NPs$_{(J)}$ with 810 nm LED lamp (1.5 W cm^{-2}). Inset: linear time data versus negative natural logarithm was obtained from the cooling period.

SQP-NPs$_{(J)}$ maintained their photothermal performance after five cycles of light on/off, suggesting good thermal stability.

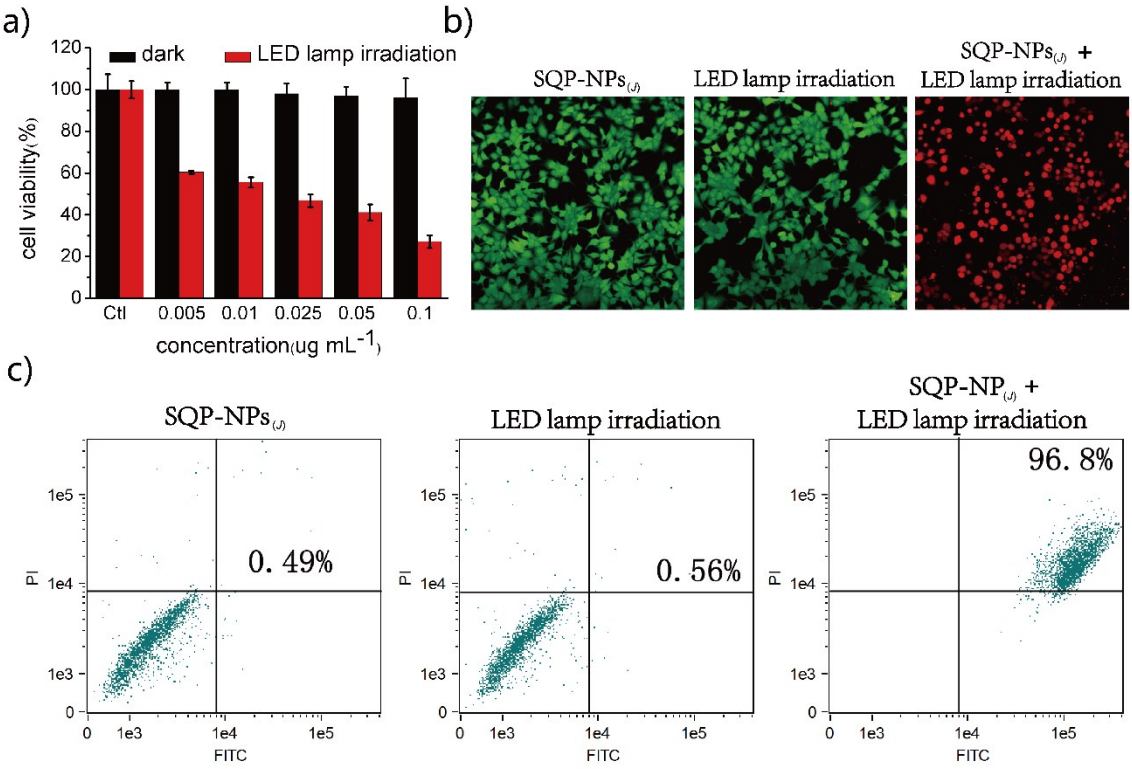

Figure S14. a) Relative viability of MCF-7 cells incubated with crescendo concentration of SQP-NPs$_{(J)}$ under dark and LED lamp (810 nm 0.8 W cm^{-2}) b) Laser Confocal Scanning Microscope (CLSM) images of calcein-AM (green fluorescence; live cells)/PI (red fluorescence; dead cells) co-stained MCF-7 cells incubated with SQP-NPs$_{(J)}$ under dark and LED lamp (810 nm 0.8 W cm^{-2}). c) Flow cytometry analysis of FITC/PI co-stained MCF-7 cells apoptosis incubated with SQP-NPs$_{(J)}$ under dark and LED lamp (810 nm 0.8 W cm^{-2}).

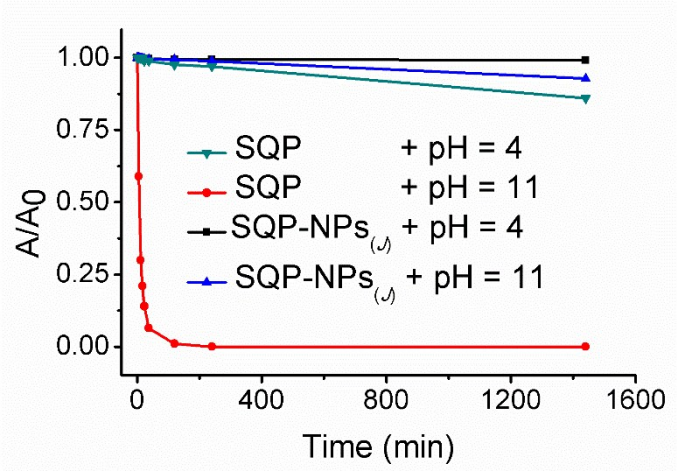

Figure S15. Changes in the absorption of SQP and SQP-NPs$_{(J)}$ upon addition of glacial acetic acid and diethylamine until the pH is 4 and 11, respectively.

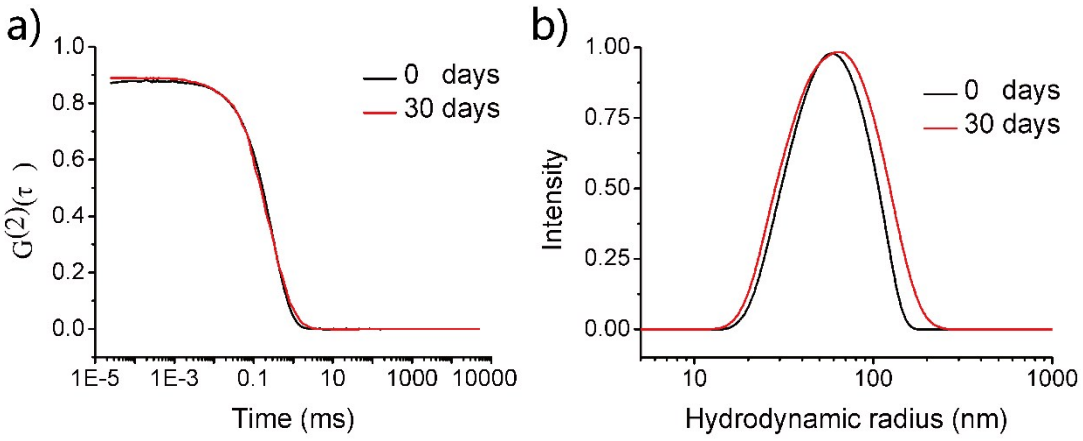

Figure S16. a) Auto correlation function obtained by DLS analysis (θ = 90º) of SQP-NPs$_{(J)}$ after stored for 30 days. b) The hydrodynamic radius ($\langle R_h \rangle$) by DLS analysis (θ = 90º) of SQP-NPs$_{(J)}$ after stored for 30 days.

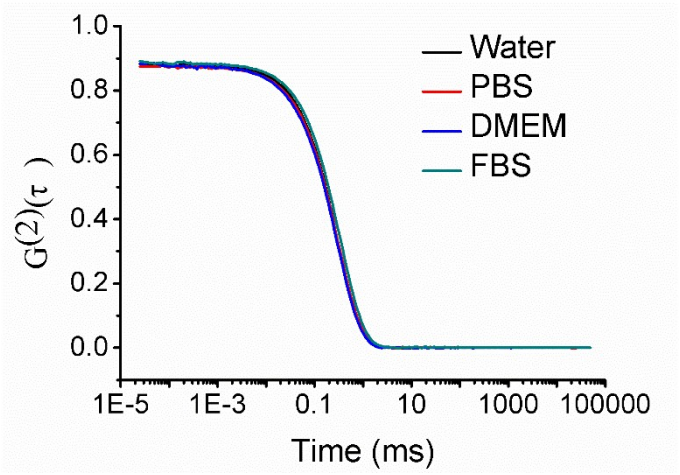

Figure S17. Auto correlation function obtained by DLS analysis (θ = 90º) of SQP-NPs$_{(J)}$ in water, PBS buffer, DMED cell culture medium, fetal bovine serum (FBS).

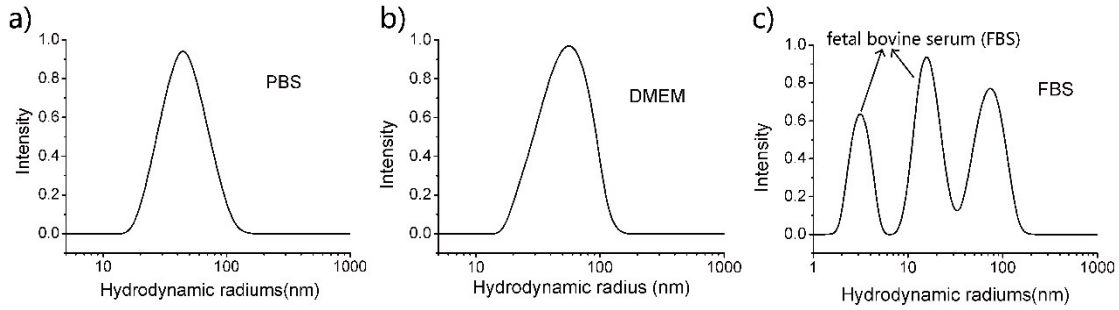

Figure S18. The hydrodynamic radius (⟨R_h⟩) by DLS analysis (θ = 90º) of SQP-NPs$_{(J)}$ in a) PBS buffer, b) DMED cell culture medium, c) fetal bovine serum (FBS).

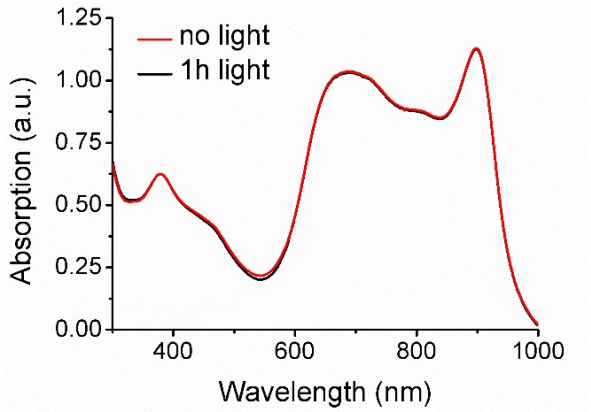

Figure S19. UV-vis-NIR absorption spectra of SQP-NPs$_{(J)}$ after exposed them under

LED lamp (808 nm 1.5 W cm^{-2}) for 1 hour.

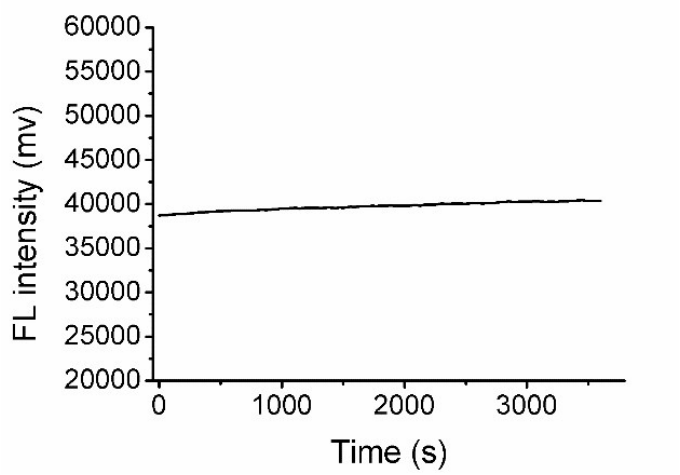

Figure S20. The FL intensity changes of SQP-$NPs_{(J)}$ when exposed them under laser (808 nm 1.5 W cm^{-2}) for 1 h.

For confirming the robust availability, a series of SQP-$NPs_{(J)}$ stability investigations were carried out. To evaluate the long-term stability of SQP-$NPs_{(J)}$, we stored the NPs for approximately 30 days in the dark. The resulting DLS measurements showed a negligible size change (Figure S16). We also incubated the SQP-$NPs_{(J)}$ in different biological fluids, and the particle size remained approximately unchanged (Figure S17 and Figure S18). In addition, we exposed them to laser irradiation (808 nm, 1.5 W cm^{-2}) for 60 minutes. The absorption spectra and emission signal at 1060 nm showed almost no changes (Figure S19 and Figure S20), proving the excellent photostability of SQP-$NPs_{(J)}$.

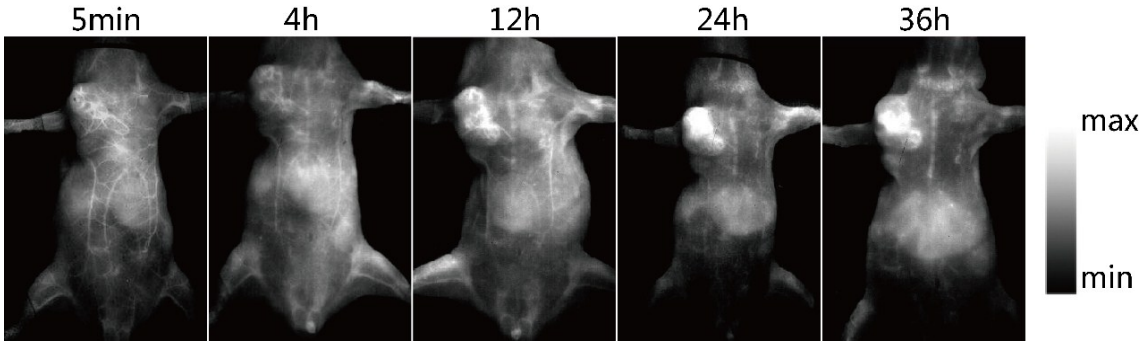

Figure S21. NIR-II fluorescence imaging of MCF-7 tumor-bearing mice after administration with 2 mg mL^{-1} $SQP\text{-}NPs_{(J)}$.

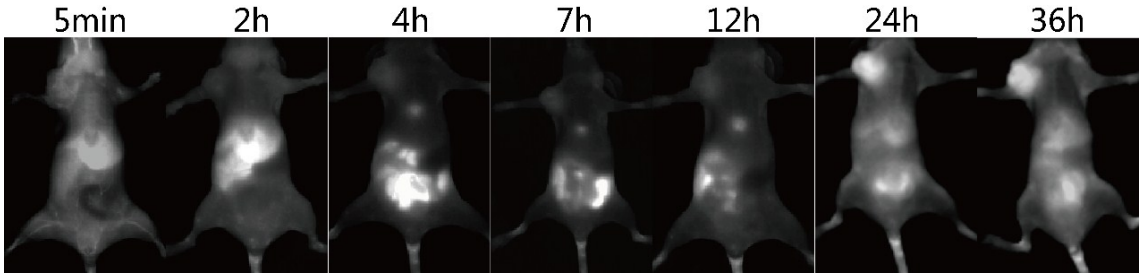

Figure S22. NIR-I fluorescence imaging of MCF-7 bearing mice after administration with ICG NPs (100 uL, 2 mg mL^{-1}).

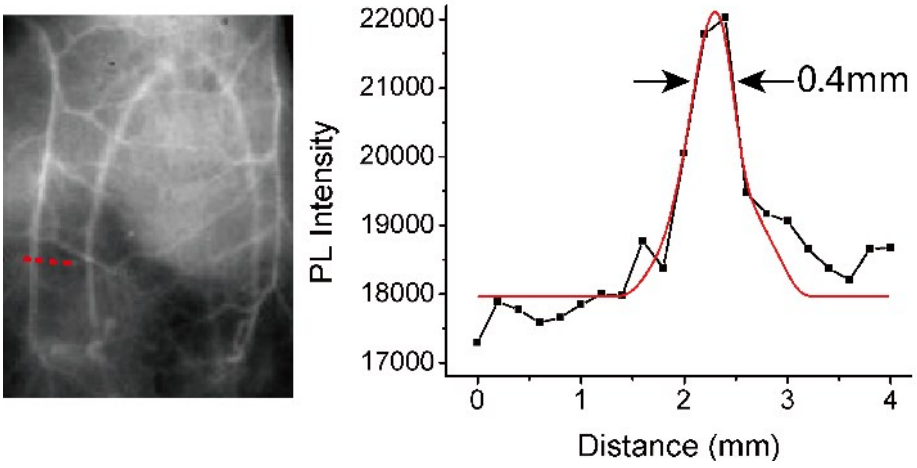

Figure S23. A cross-sectional fluorescence intensity profiles along red-dashed lines of the mouse injected with $SQP\text{-}NPs_{(J)}$ and the vessel width analysis.

Notably, the blood vessels with a diameter less than 0.4 mm could be clearly detected, evidencing the high degree of resolution generated by the NIR-II imaging combined with SQP-NPs$_{(J)}$.

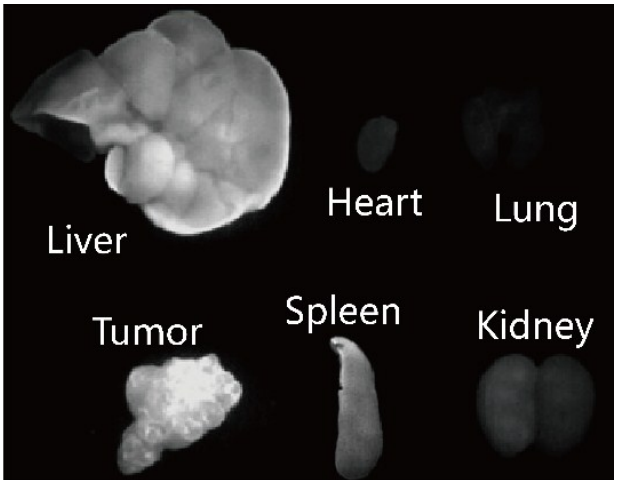

Figure S24. *Ex vivo* NIR-II fluorescence imaging of main organs after 36 h intravenous administration of SQP-NPs$_{(J)}$ (100 uL, 1 mg mL^{-1}).

Many SQP-NPs$_{(J)}$ accumulated in the spleen and liver, evidencing that the clearance route of SQP-NPs$_{(J)}$ is mainly through the hepatobiliary system.[3]

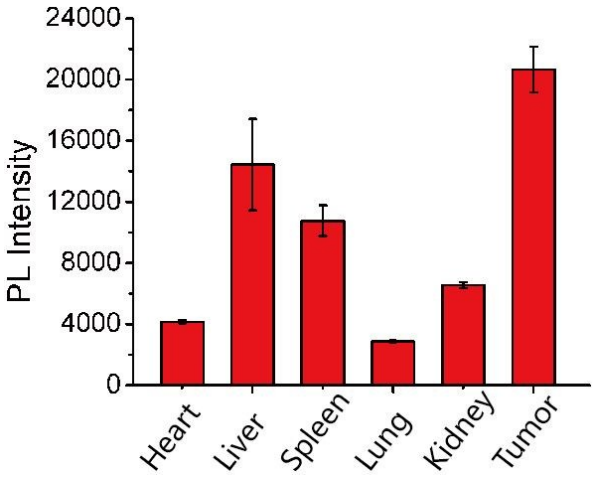

Figure S25. Quantitative NIR-II fluorescence intensity of main organs.

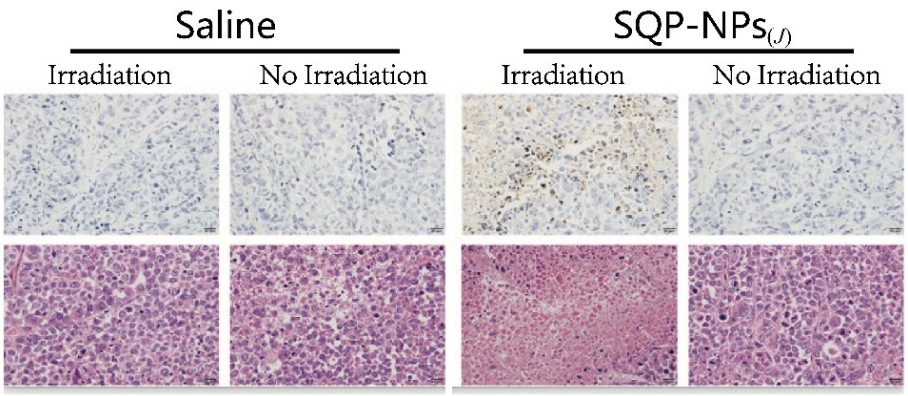

Figure S26. H&E staining in tumor sites of MCF-7 tumor-bearing nude mouse with different treatments.

After 24 h of treatment, the control group tumor sections showed no obvious tissue denaturation (i, ii, iii), but the tumor cells collected from the SQP-NPs$_{(J)}$ group (iv) were nearly all damaged after the irradiation.

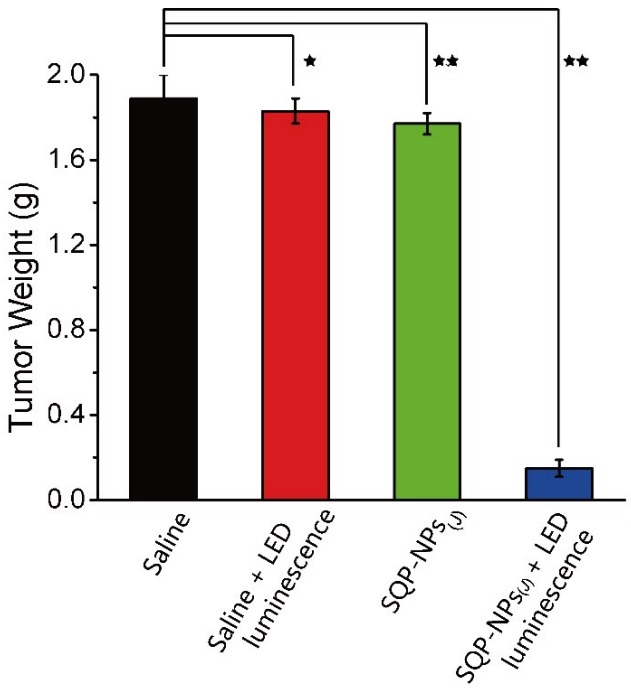

Figure S27. Tumor weight from different groups of MCF-7 tumor-bearing mice after therapy for 14 days.

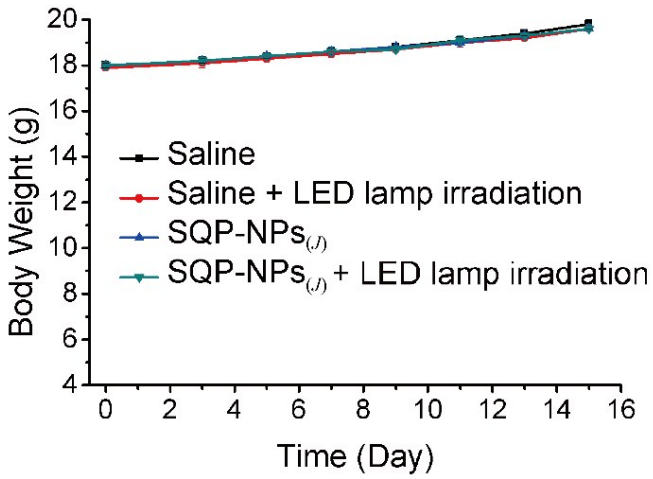

Figure S28. Body weight of the MCF-7 tumor-bearing mice after different groups of therapy with the change of time.

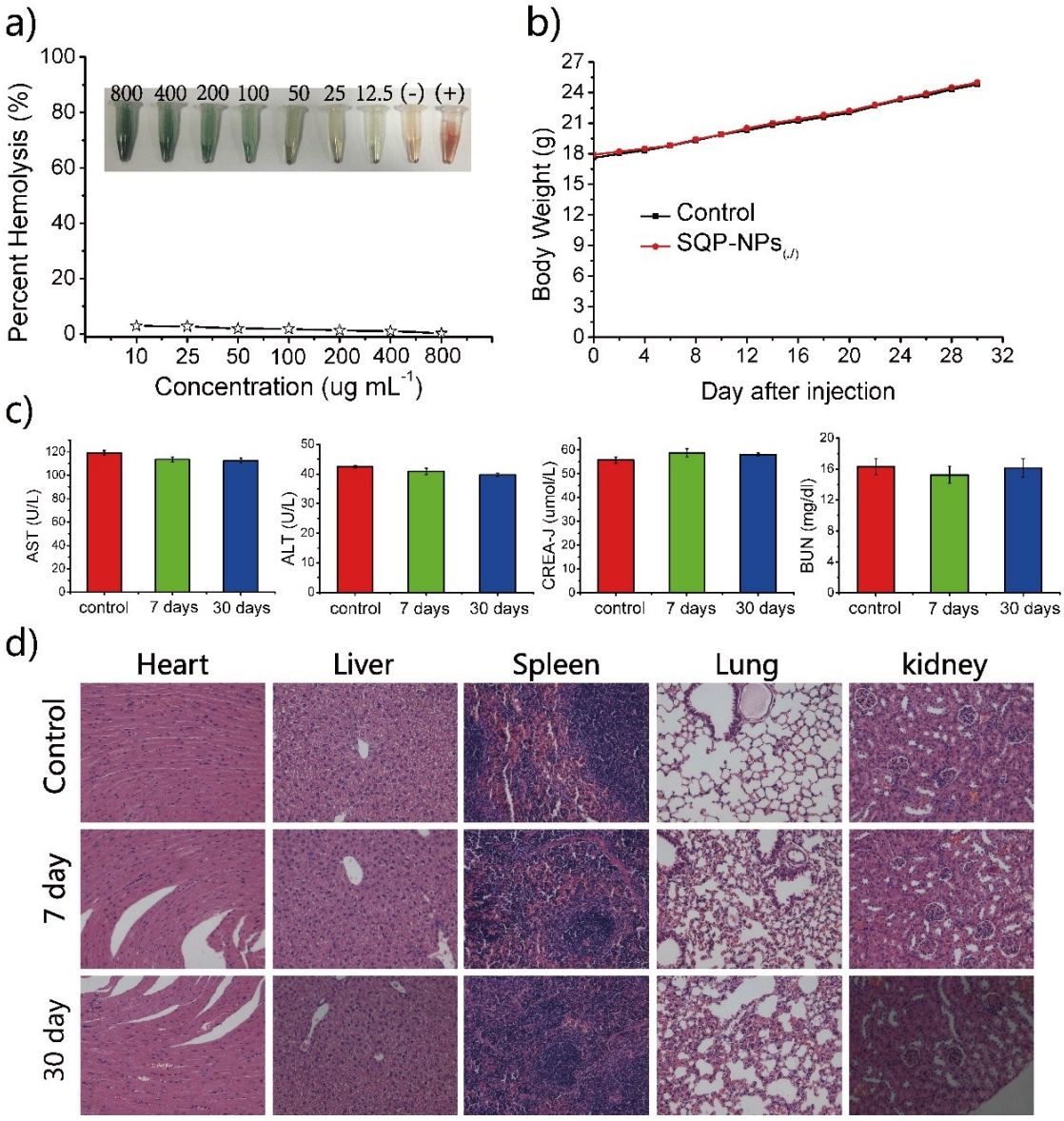

Figure S29 a) *In vitro* hematoxylin analysis by RBCs incubating with SQP-NPs$_{(J)}$ at different concentration. Deionized water served as positive controls (+) and PBS served as negative controls (-). Inset: Image of hematoxylin results. b) Body weight curve of the mice that treated with SQP-NPs$_{(J)}$ during 30 days. c) Blood chemistry analysis of healthy mice after injected with SQP-NPs$_{(J)}$ at 0, 7, 14 and 30 days. d) Hematoxylin and eosin (H&E) co-stained histological analysis of several organs from four groups: control, 7, 14, 30 days.

To evaluate in vitro hemolytic activities between SQP-NPs$_{(J)}$ and blood components, we monitored the UV-vis absorption spectra at approximately 541 nm to detect whether RBCs were damaged by various concentration of SQP-NPs$_{(J)}$. As shown in Figure S29a, the percent hemolysis was calculated and the value was within the limits of 5%, indicating the good blood biocompatibility of SQP-NPs$_{(J)}$. Figure S29b showed that the body weight curves of the treated mice have no disparity compared to the mice treated with saline, indicating that SQP-NPs$_{(J)}$ have minimal impact on mouse growth. Figure S29c shows that the hepatic and renal function of the treated mice was not adversely impacted. As we can see from the H&E stained histological images (Figure S29d), the viscera organs, including the heart, liver, spleen, lung and kidney, showed no obvious cell damage or pathological inflammatory changes by optical microscope within 30 days.

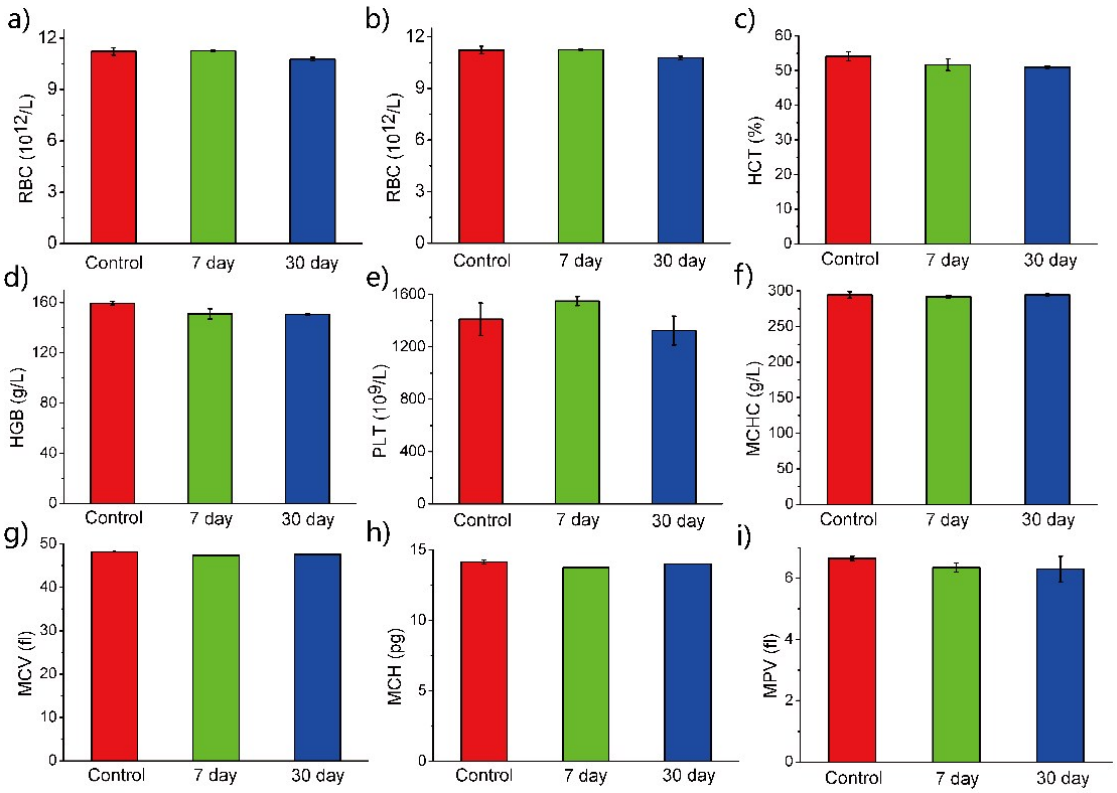

Figure S30. Blood routines of mice examination were measured after the treatment with SQP-NPs$_{(J)}$ (2 mg mL^{-1}, 100 uL) during 30 day.

The blood cell analyses showed that all blood cell indicators were within normal limits 30 days after the mice were injected with SQP-NPs$_{(J)}$.

REFERENCES

(1) Lyu, Y.; Xie, C.; Chechetka, S. A.; Miyako, E.; Pu, K. Y. Semiconducting polymer nanobioconjugates for targeted photothermal activation of neurons. *J. Am. Chem. Soc.* **2016**, 138, 9049-9052.

(2) Lynch, D. E.; Geissler, U.; Byriel, K. A. An investigation into the electrical conduction properties of poly(oligo(1-methylpyrrol-2-yl)Squaraine)s. *Synthetic Metals*. **2001**, 124, 385-391.

(3) Xie, C.; Zhen, X.; Miao, Q. Q.; Lyu, Y.; Pu, K. Y. Self-assembled semiconducting polymer nanoparticles for ultrasensitive near-infrared afterglow imging of metastatic tumors. *Adv. Mater.* **2018**, 30, 1801331.